



# Tunable multiple-passband microwave photonic filter based on external optical injected Fabry-Pérot laser

WENXUAN WANG,<sup>1</sup> LONG HUANG,<sup>1</sup> JI TAO,<sup>1</sup> HUATAO ZHU,<sup>2</sup> XINWEI DU,<sup>3</sup> LIJUN HAO,<sup>1</sup> CHANGYUAN YU,<sup>3</sup> AND XIANGFEI CHEN<sup>1\*</sup>

<sup>1</sup>Key Laboratory of Intelligent Optical Sensing and Integration, College of Engineering and Applied Sciences, Nanjing University, Nanjing 210009, China

<sup>2</sup>College of Information and Communications, National University of Defense Technology, Wuhan 430010, China

<sup>3</sup>Department of Electronic and Information Engineering, The Hong Kong Polytechnic University, Hung Hom, Hong Kong

\*chenxf@nju.edu.cn

**Abstract:** This paper proposes a tunable multiple-passband microwave photonic filter (MPF) that is incorporated with an injection-locked Fabry-Pérot (FP) laser. In the proposed MPF, multiple passbands can be easily generated based on the frequency-selection effects of the laser structure in the case of multiple light waves injection. The novelty here is that the obtained multiple-passband MPF can achieve either a dual-passband or a single-passband by using merely one experimental scheme. Moreover, since the laser injection ratio of the proposed scheme is high, the central frequency of each passband has a large tunable range. More tunable passbands can be generated by employing more external wavelengths. By fine-tuning the injection parameters, the frequency tuning range of 17 GHz and the out-of-band rejection ratio of 24.1 dB are achieved for the dual-passband MPF, and the out-of-band rejection ratio of 22 dB and the 3-dB bandwidth of 360 MHz are achieved for the single-passband MPF. In addition, the attained peak power and bandwidth of the proposed MPF are investigated with respect to the injection parameters, including detuning frequency, injection ratio and bias current of FP laser. The stability and dynamic range of the MPF are also evaluated through experiments.

© 2019 Optical Society of America under the terms of the [OSA Open Access Publishing Agreement](#)

## 1. Introduction

Microwave photonic filter (MPF) has attracted much research attention due to the utilization of microwave photonics technologies, which offers significant advantages of electromagnetic interference immunity, broad bandwidth and low dispersion [1,2]. The MPF with high quality factor or narrow bandwidth can provide high frequency selectivity, spectral purity, resolution and bandwidth to overcome the limitations of electronic approaches [3]. Due to these advantages, the MPF is a significant component for optoelectronic oscillators (OEO) [4], microwave signal measurements [5,6] and target identification radar systems [7], etc. Recently, to meet the increasing demand for multiband or multifunction filters, many approaches have been proposed to realize multiple-passband MPFs [4,8–12]. The use of MPFs can prevent multiple cascaded filters and provide promising OEO applications in the microwave photonic sensor system [4]. However, most of the multiple-passband MPFs have the fixed passbands or the limited tunable range [10–12].

One of the commonly used multiband MPFs is implemented using a tapped-delay-line structure with the finite impulse response (FIR) [8,13]. However, since the periodic spectral response of the FIR may lead to the spectral overlapping, the processing frequency has to be a fraction of free spectral range (FSR). If FIR is replaced by infinite impulse response (IIR), the numbers of taps will also determine the width of the passbands, the tunability is limited by the

time delay and the stability is poor. Another approach to implement the MPF is based on a sliced broadband source combined with a dispersive element or a spectrum slicer, such as the standard single mode fiber or a Mach-Zehnder Interferometer (MZI) [9,14,15]. Nevertheless, since the spectrum slicer that consists of various optical components is complicated and the MZI is extremely sensitive to environment disturbances [7,9], the broadband source is not commonly used for communications [14]. In most of the approaches, the MPFs are realized by phase-shifted fiber Bragg grating (PS-FBG) or equivalent phase-shifted fiber Bragg grating (EPS-FBG) [10,16,17]. In [10], the authors convert phase-modulation (PM) into intensity-modulation (IM) through two notches at the  $\pm 1$ st channels of the EPS-FBG. However, the beating note will fall out of the desired frequency because of the small spacing between the two passbands. This will cause a more limited tunable range of the multiband MPF compared with other schemes. In addition, the scheme in [3] uses a stimulated Brillouin scattering (SBS) assisted filter incorporated in the system for carrier suppression, which significantly increases the system cost and complexity. In [12,17], a dual-passband or multiple-passband MPF is proposed based on a PS-FBG or multi-channel PS-FBG, which uses two orthogonal polarized optical waves or multiple PS-FBGs to realize multiband. The corresponding performance of the frequency tuning range and the stability are restricted due to the reflection responses of the FBG. Many approaches have been proposed to map an optical filter by using the Fabry-Pérot cavity, such as the FP laser [18] and the Fabry-Perot semiconductor optical amplifier (FP-SOA) [19,20]. Both of FP laser and FP-SOA have the active cavity that can amplify multiple input optical signals, since FP cavity possesses multiple modes. However, the single optoelectronic oscillator (OEO) proposed in [18] is based on an intensity modulator and an FP laser, which has the limited frequency tunability of 4.44 GHz. In [19], the authors proposed to use two tunable lasers and an FP-SOA, by adding the microwave frequency responses with dual-wavelength injection together in their passbands, a single-passband MPF can be generated. A tunable MPF is proposed in [20], whose tunability and the number of passbands are determined by the spectrum deviation of optical carrier and two longitudinal-mode peaks. The tunability of the MPFs in [19,20] can merely be realized by adjusting the bias current of FP-SOA. Here, we aim to propose a new approach to implement the multifunctional MPF with both a single-passband and a multiple-passband. Furthermore, the proposed MPF has a wide tunable frequency range and simple structure which reduces the complexity and cost of the system.

In this paper, we propose and experimentally demonstrate a simple multiple-passband MPF with wide tunable frequency range, based on an injection-locked Fabry-Perot laser. It is designed based on the wavelength selective amplification effect of an FP laser with multiple longitudinal modes under external optical injection. The FP laser used as the slave laser, is mode-locked by the multiple modulated optical signals which couple the lightwaves from multiple tunable lasers (TL), and the lower sidebands of the modulated signals can be resonantly amplified by the multiple cavity modes. We carry out the experiments by incorporating two tunable lasers. By using the same experimental scheme, we can achieve the multiple-passband filter with either a single-passband or a dual-passband. The frequency response of the proposed MPF can be controlled by the injection parameters, including detuning frequency, injection ratio and bias current of the FP laser. In the experiment, the central frequency tuning range of each passband of 17 GHz, the out-of-band suppression of 24.1 dB, and the shape factor of the 1st passband of 2.9 can be achieved for the dual-passband MPF. The shape factor of 3.7 and the insertion loss of 22 dB are achieved for the single-passband MPF. For the dual-passband MPF, the stability is investigated. The fluctuations of the central frequency and the magnitude of the 1st passband are within  $\pm 29$  MHz and  $\pm 0.14$  dB, and those of the 2nd passband are within  $\pm 43$  MHz and  $\pm 0.27$  dB, respectively. As far as we know, stronger injection ratio expands the locking range [18]. In the proposed scheme, the injection ratio is beyond 15 dB which is higher than other existing solutions and no device is

required to amplify the optical or electronic signal. In addition, the structure is simple and compact, which is suitable for integrating on a chip.

## 2. Principle

The principle of the proposed MPF based on an optical injection-locked (OIL) Fabry-Perot laser is shown in Fig. 1(a). The solid line indicates the optical path and the dotted line indicates the electrical path. There are multiple tunable lasers named as master lasers (ML), which emit continuous wave lights into the electro-optic modulator (EOM) driven by the radio frequency (RF) signal. The polarization controllers (PC) are incorporated to adjust the polarization states between the MLs and the EOM.

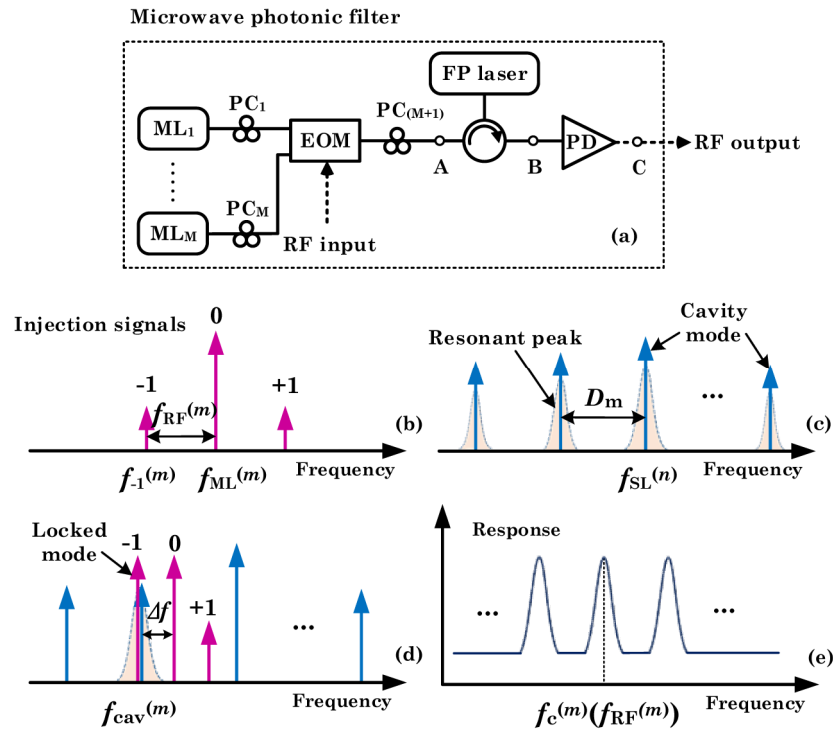


Fig. 1. (a) Schematic diagram of the proposed MPF. (ML: master laser. PC: polarization controller. EOM: electro-optic modulator. PD: photodetector) (b) Injection signals modulated by the *m*th master laser. (c) FP laser spectral response. (d) Injection-locked Output under the *m*th master laser. (e) Frequency response of the multiple-passband MPF.

Taking the *m*th ML (ML<sub>*m*</sub>) for example, the frequencies of ML<sub>*m*</sub> and FP laser are denoted by  $f_{ML}^{(m)}$  and  $f_{SL}^{(n)}$  ( $m = 1, 2, \dots, M; n = 1, 2, 3, \dots$ ), respectively. The signal at point A before injection consists of a strong carrier and two sidebands ( $\pm 1$ st order) [21] as shown in Fig. 1(b). The frequency difference between the carrier ( $f_{ML}^{(m)}$ ) and the  $\pm 1$ st order sideband ( $f_{\pm 1}^{(m)}$ ) is equal to the RF frequency ( $f_{RF}^{(m)}$ ). The EOM is connected to an FP laser via a PC and a circulator. The multi-longitudinal cavity modes of FP laser are equally spaced as shown in Fig. 1(c), with the mode spacing denoted as  $D_m$ . The injection signals around the cavity modes are amplified because of the cavity enhancement of FP resonator. This phenomenon can be usually regarded as the periodic resonant peaks centered at the red-shifted cavity modes under external injection [7,20,22]. The power spectrum of the signal at point B is shown in Fig. 1(d). If  $f_{-1}^{(m)}$  is within the range of a gain, the FP laser will be locked by the resonantly amplified  $-1$ st order sideband when enough amplification is obtained depending on the injection parameters. When  $f_{-1}^{(m)}$  equals the frequency of the red-shifted cavity mode

( $f_{cav}^{(m)}$ ), the sideband will obtain the highest power close to the carrier. Only the  $-1$ st order sideband will obtain high conversion efficiency while the other sidebands cannot be affected strongly. Furthermore, the combined optical signal after FP laser which originates from the multiple ML sources can be written as

$$E(t) \approx \sum_{m=1}^M \sqrt{G(\omega_{ML}^{(m)})} J_0(\beta) \cos \omega_{ML}^{(m)} t \\ + \sum_{m=1}^M \sqrt{G(\omega_{ML}^{(m)} + \omega_{RF}^{(m)})} J_0(\beta) \cos(\omega_{ML}^{(m)} + \omega_{RF}^{(m)}) t \\ + \sum_{m=1}^M \sqrt{G(\omega_{ML}^{(m)} - \omega_{RF}^{(m)})} J_0(\beta) \cos(\omega_{ML}^{(m)} - \omega_{RF}^{(m)}) t, \quad (1)$$

where  $\omega_{ML}^{(m)}$  is the angular frequency of the  $m$ th ML,  $\omega_{ML}^{(m)} = 2\pi f_{ML}^{(m)}$ ,  $\beta$  is the phase modulation index of the EOM,  $J_n$  is the  $n$ th order Bessel function of the first kind, and  $G(\omega)$  represents the effective gain of the FP laser with periodic resonant peaks, as shown in Fig. 1(c). At the output of the photonic detector (PD), one gain spectrum of the FP laser is mapped to one passband. At the point C (Fig. 1(d)), we obtain the multiple-passband response with the central frequency of  $f_c^{(m)}$  or  $f_{RF}^{(m)}$

$$H(\omega_{RF}) = \frac{V_{out}}{V_{in}} \approx \sum_{m=1}^M \frac{R \sqrt{G(\omega_{ML}^{(m)})} J_0(\beta) J_1(\beta) (\sqrt{G(\omega_{ML}^{(m)} + \omega_{RF}^{(m)})} + \sqrt{G(\omega_{ML}^{(m)} - \omega_{RF}^{(m)})})}{\beta V_\pi}, \quad (2)$$

where  $R$  is a parameter related to the responsivity and the load impedance of the PD, and the path losses and  $V_\pi$  is the half-wave voltage of the EOM.

We further provide a detailed investigation on the tunability of these passbands. The slave laser injected by external light can be described by rate equations [23–25] which modify the free-running laser equation within the framework of the classic semiconductor laser theory proposed by Lamb [26] in 1965. By applying the small-signal linear approximation and stability analysis to the rate equations, it is concerned about the steady locking range which is shown as the detuning angular frequency and expressed as

$$-k_{inj} \sqrt{1 + \alpha^2} \frac{A_{in}}{A_S} \leq \Delta\omega \leq k_{inj} \frac{A_{in}}{A_S}, \quad (3)$$

where  $A_{in}$  and  $A_S$  are the normalized and the steady-state value of electric field amplitude of the master laser,  $\alpha$  is the linewidth enhancement factor,  $k_{inj}$  named as the injection coupling coefficient has relation to the ratio of external optical injection to intra-cavity laser and the time that the light travels back and forth inside the cavity once time. In the literature, taking account to the injection ratio  $R$ , which defined as the injected power and the emitting power of the external cavity of the FP laser,  $R = (A_{in}/A_S)^2$ , Eq. (3) can be rewritten as

$$-k_{inj} \sqrt{1 + \alpha^2} \sqrt{R} \leq \Delta\omega \leq k_{inj} \sqrt{R}. \quad (4)$$

Furthermore, derivation from [27], the central angular frequency of the  $m$ th passband ( $\omega_c^{(m)}$ ) is equal to the resonance frequency between the master laser and the red-shifted cavity mode of the slave laser, namely:

$$\omega_c^{(m)} = -\frac{1}{2} \alpha g (N_S - N_{th}) + \Delta\omega^{(m)} \\ = -k_{inj} \frac{A_{in}^{(m)}}{A_S} \sin \phi_S = -k_{inj} \sqrt{R^{(m)}} \sin \phi_S, \quad (5)$$

where  $g$  is the linear gain coefficient,  $N_S$  and  $N_{th}$  are the carrier density in steady-state and the threshold carrier just as the loss is equal to the gain, and  $\Delta\omega^{(m)}$  also refers to the resonance frequency enhancement. Here we define that

$$\Delta\omega^{(m)} = \omega_{ML}^{(m)} - \omega_{SL}^{(m)}, \Delta f^{(m)} = f_{ML}^{(m)} - f_{SL}^{(m)}, \quad (6)$$

$$R^{(m)} = 20 \log \left( \frac{A_{in}^{(m)}}{A_S} \right) = 10 \log \left( \frac{P_{in}^{(m)}}{P_S} \right) \text{ (dB)}. \quad (7)$$

In Eq. (5),  $\omega_c^{(m)}$  is related to  $\Delta f^{(m)}$ ,  $R^{(m)}$  and  $I_b$ . The detuning frequency  $\Delta f^{(m)}$  is defined as the frequency difference between the  $m$ th master laser and the longitudinal mode of the free-running FP laser, and the bias current makes an effect on the output power of the FP laser directly. If the aforementioned parameters can be tuned on the large scale, the multiple passbands of the proposed MPF have a wide tunability. However, due to the limitation of experimental conditions, we carried out the experiment incorporating two MLs with at most two passbands.

### 3. Experimental setup

According to the analysis given in section II, a proof-of-concept experiment shown in Fig. 2 is performed. Two lightwaves are emitted from TL1(Santac, TSL-210) and TL2(Agilent, 81989A) with output powers of 7 dBm and 8 dBm, respectively, which are limited by the instrument performances. They are coupled with PC and OC and then sent to the PM (EOspace, PM-DV5-40-PFU-PUF-LV, 40GHz,  $V_\pi = 5V$ ). By tuning PC1 and PC2, the polarization states of two input optical sources are aligned with the PM. A vector network analyzer (VNA) is used to acquire the frequency response of MPF, which can import the microwave signal into PM as well as a sweep from 0 to 50 GHz with a stable magnitude. The modulated signal is injected into the slave FP laser through an optical circulator (OC). The polarization direction of the injected light is matched with that of the FP laser using the PC3. PC3 is adjusted to align the polarization of the injection light to the FP laser. The FP laser diode is controlled by a laser diode controller (Thorlabs, LDC 205C) and a temperature controller (Thorlabs, TED 200C). The threshold current of the FP laser diode is 12mA. The output lightwave of the FP laser diode is routed by the OC and divided into two parts. 1% portion is connected to an OSA (Yokogawa, AQ6370), and 99% portion is directed to a PD (u2t XPDV2120R) for optical-to-electrical conversion. The bandwidth and the responsivity of the PD are 50 GHz and 0.65 A/W, and the frequency resolution of OSA is 0.02 nm.

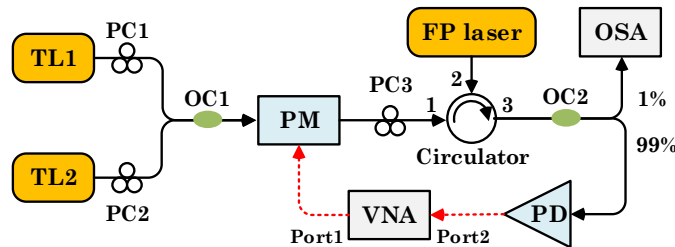


Fig. 2. Experimental setup of the proposed MPF. (TL: tunable laser. PC: polarization controller. OC: optical coupler. PM: phase modulator. FP: Fabry-Perot laser. OSA: optical spectrum analyzer. PD: photodetector. VNA: vector network analyzer.)

In our experiment, the FP laser operates in the C band, and the mode spacing  $D_m$  is about 1.34 nm. The two other tunable lasers also play important roles in this experiment, that TL1 works in short wavelength range and generates a low-frequency response which composes the first passband, and similarly TL2 works in long wavelength range and generates a high-

frequency response which forms the second passband. Considering the injection ratio and the detuning frequency of TL1 and TL2 according to Eq. (6) and (7), we have

$$\Delta f_1 = f_{ML}^{(1)} - f_{SL}^{(1)}, \Delta f_2 = f_{ML}^{(2)} - f_{SL}^{(2)}, \quad (8)$$

$$R_1 = 10\log\left(\frac{P_m^{(1)}}{P_s^{(1)}}\right), R_2 = 10\log\left(\frac{P_m^{(2)}}{P_s^{(2)}}\right). \quad (9)$$

$\Delta f_1$  is the detuning frequency as the frequency difference between the first master laser and the first longitudinal mode of FP laser, and  $R_1$  is the injection ratio as the power ratio between them. There is the same definition for the second master laser and the second longitudinal mode of FP laser.

## 4. Results and discussions

### 4.1 Dual-passband

In the experiment, the wavelengths of two light waves from TL1 and TL2 are set at 1549.192 and 1562.730 nm, respectively. When  $I_b = 25.14$  mA,  $R_1 = 24.38$  dB,  $R_2 = 18.09$  dB,  $\Delta f_1 = 16.00$  GHz, and  $\Delta f_2 = 18.90$  GHz in Fig. 3 that the dual-passbands are centered at 13.3 and 20.7 GHz and the out-of-band rejection ratio is 24.1 dB better than [9,13,18]. It is proved that a stable dual-mode operation with a large suppression ratio has been achieved by OIL. By defining as the ratio of the 20- and 3-dB bandwidths, the shape factor of 2.9 and 4.8 for the 1st and 2nd passband are exhibited. The insets of the zoom-in view show the 3-dB bandwidths of two passbands are 496 and 590 MHz, respectively, and the amplitude of each passband is about  $-22.8$  dB.

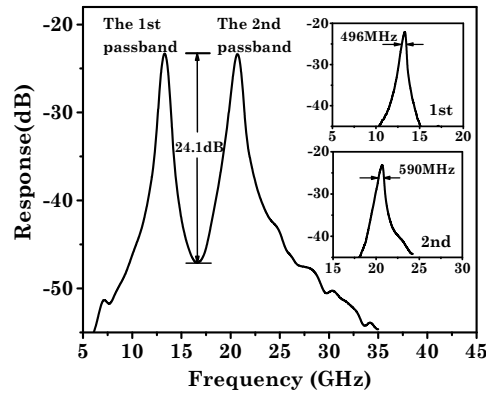


Fig. 3. Spectral response of the dual-passband MPF and the zoom-in view of the two passbands.

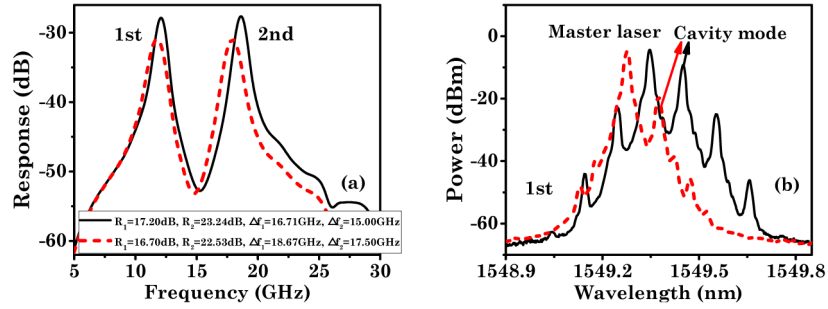


Fig. 4. (a) Measured amplitude responses of the dual-passband MPFs realized under different conditions (b) the 1st passband corresponding optical spectra.

It shows the different frequency responses of dual-passband MPFs under the same  $I_b$  of 26.40 mA in Fig. 4(a). The black solid line and the red dashed line represent the different stable-locking states by setting different  $\Delta f$  and  $R$ . For both passbands, the central frequency, out-of-band suppression, and peak amplitude are significantly decreased when increasing  $\Delta f$  and decreasing  $R$  at the same time. Conversely, the 3-dB bandwidth gets larger.

In addition, the corresponding optical spectrum of the first passband is shown in Fig. 4(b). The magnitude of the cavity mode labeled with the red dashed line is decreased worse because the gain spectrum reduces with  $\Delta f$  and  $R$ . Here,  $\Delta\lambda$  is defined as the wavelength difference between the master laser ( $\lambda$ ) and the longitudinal mode of FP laser ( $\lambda_{FP}$ ). Denoting  $\Delta\lambda = \lambda - \lambda_{FP}$ , the central frequency of the MPF response can be calculated as  $f_c = c\Delta\lambda/\lambda^2$  [22]. Take the 1st passband of the black solid line for an example, as  $\lambda_1 = 1549.346$  nm and  $\lambda_{FP1} = 1549.443$  nm observed in Fig. 4(b),  $f_{c1} = 12.123$  GHz can be calculated by the above formula. It is close to the central peak at the frequency of 12.072 GHz measured in Fig. 4(a). Therefore, if we set  $\Delta f$  and  $R$  properly, a dual-passband MPF with high gain, large out-of-band suppression ratio and wide tunability centered at the desired frequency can be achieved.

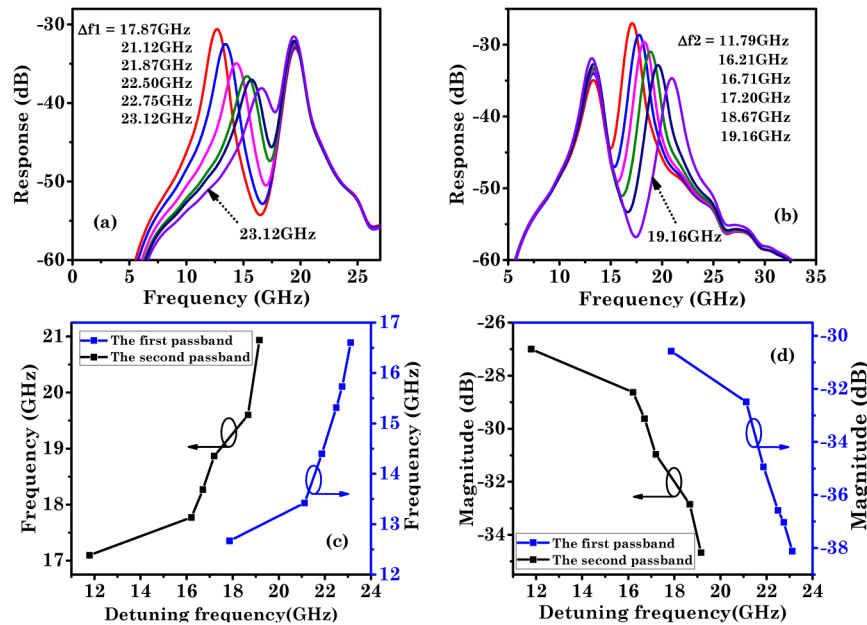


Fig. 5. Measured amplitude responses of the dual-passband MPFs. (a) The 1st passband is tuned with  $\Delta f_1$ . (b) The 2nd passband is tuned with  $\Delta f_2$ . (c) The relationship between the detuning frequency and the central frequency of each passband. (d) The relationship between the detuning frequency and the magnitude of each passband.

The experimental results shown in Fig. 5, Fig. 6 and Fig. 7 illustrate the change regulation between the frequency response of MPF and the tunable parameters. Firstly, Fig. 5(a) shows the amplitude responses of the MPFs achieved by tuning  $\Delta f_1$  from 17.87 to 23.12 GHz, while  $I_b = 25.14$  mA,  $R_1 = 24.38$  dB,  $R_2 = 18.09$  dB,  $\Delta f_2 = 19.87$  GHz and the 2nd passband with a central frequency of about 19.5 GHz kept unchanged. Then, Fig. 5(b) shows the amplitude responses of the MPFs achieved by tuning  $\Delta f_2$  from 11.79 to 19.16 GHz, while  $I_b = 25.14$  mA,  $R_1 = 24.38$  dB,  $R_2 = 18.09$  dB, and  $\Delta f_1 = 16.00$  GHz. Moreover, the 1st passband with a central frequency of about 13.3 GHz is kept unchanged and the 2nd passband is tuned by changing the wavelength of TL2 with a tuning step of 0.006 nm. The central frequency and magnitude as a function of detuning frequency are demonstrated in Figs. 5(c) and 5(d), respectively. As shown in these figures, the central frequency increases with the increase of the detuning frequency. And according to Eq. (5), the central frequency of each passband can be increased by increasing  $\Delta f$ . The measurement results agree well with the theoretical analysis and mathematical representation in section II. Meanwhile, the magnitude decreases along with the growing detuning frequency because of the out-of-band rejection ratio increment while the shape of the other passband is almost unchanged.

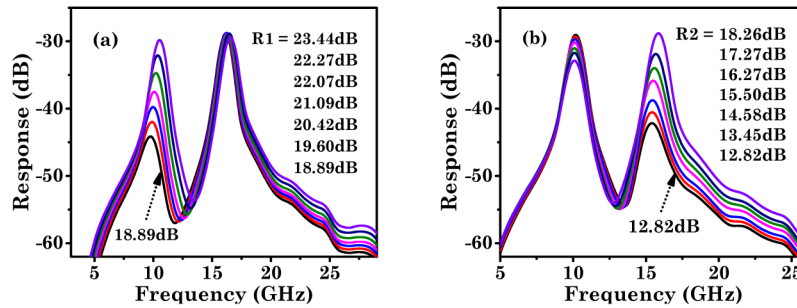


Fig. 6. Measured amplitude responses of the dual-passband MPFs. (a) The 1st passband is tuned with  $R_1$ . (b) The 2nd passband is tuned with  $R_2$ .

To illustrate the independent tunability with the injection ratio of the dual-passband, when  $I_b = 25.85$  mA,  $R_2 = 16.46$  dB,  $\Delta f_1 = 13.10$  GHz, and  $\Delta f_2 = 15.23$  GHz, we firstly fix the central frequency of the 2nd passband at 16.3 GHz and the central frequency of the 1st passband is shifted from 9.7 to 10.5 GHz by tuning  $R_1$  from 23.44 to 18.89 dB, and the result is shown in Fig. 6(a). Then when  $I_b = 25.72$  mA,  $R_1 = 20.43$  dB,  $\Delta f_1 = 12.00$  GHz, and  $\Delta f_2 = 14.74$  GHz, we fix the central frequency of the 1st passband at 10.1 GHz and the central frequency of the 2nd passband is tuned from 15.3 to 16.8 GHz by tuning  $R_2$  from 18.26 to 12.82 dB, and the result is shown in Fig. 6(b). In Figs. 6(a) and 6(b), the resonance frequency and peak value both increase with the increasing injection ratio. The same principle as Fig. 5 that  $\omega_c$  is proportional to the external power injection ratio. Moreover, according to Eq. (4), the range of the detuning frequency or resonance frequency enhancement is increased with the increment of injection ratio, and the maximum value expressed as  $\Delta\omega_{max} = k_{inj} \sqrt{R}$ . So, it illustrates the trend that strong optical injection locking ( $R > 10$  dB) can broaden the stable locking range. Most of the measurement results are obtained under a large optical injection ratio, however, the external power of optical injection is in the range of  $-3$  dB to  $-5$  dB.

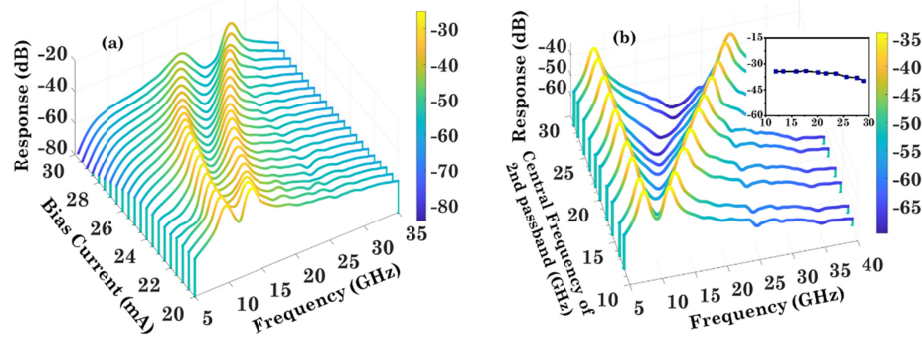


Fig. 7. (a) Measured amplitude responses of the dual-passband MPFs realized by tuning  $I_b$ . (b) Amplitude responses of the generated MPFs that the 2nd passband coarsely tuned from 11.9 GHz to 28.9 GHz. The inset is the variation of response peak values.

By injection from a master laser, the frequencies of the master and slave are fixed. Changing the slave bias current will lead to the change of the locked conditions, thus causing the shift of the phase difference between the master and the slave. Figure 7(a) shows the measured amplitude responses of the MPFs realized by tuning  $I_b$  from 22 to 28 mA with 1 mA step when  $\Delta f_1 = 16.00$  GHz,  $\Delta f_2 = 18.671$  GHz,  $R_1 = 24.38$  dB, and  $R_2 = 18.09$  dB. As a result of the gain spectrum shape of the FP laser changed with the number and distribution of carriers which is determined by the number of injection photons, the response shape can be changed. Meanwhile, the peak response values of two passbands varied along with  $I_b$ , both increase at first and then decrease. Besides, there are the same current differences but the different interval of the central frequency namely the tuning of  $f_c$  is not proportional to the tuning of  $I_b$ .

From Fig. 7(b), the 1st passband with the central frequency of 8 GHz and the amplitude about  $-34$  dB is kept unchanged, then the 2nd passband is tuned by tuning the wavelength and power of TL2 and the bias current of FP laser together. It can be achieved that the central frequency of the 2nd passband is tuned from 11.9 GHz to 28.9 GHz with a step about 2 GHz. The independently tunable range of 17 GHz is larger than other solutions [13,14,18]. When the difference of the two passbands increases, the amplitude of the 2nd passband drops slightly in the inset figure, but the out-of-band suppression ratio can be maintained above 30 dB, which is much more than the results shown in [9,13,14,18]. Limited by the adjustable range of output power and wavelength of TLs in our experiment, a larger tunable range should be achieved.

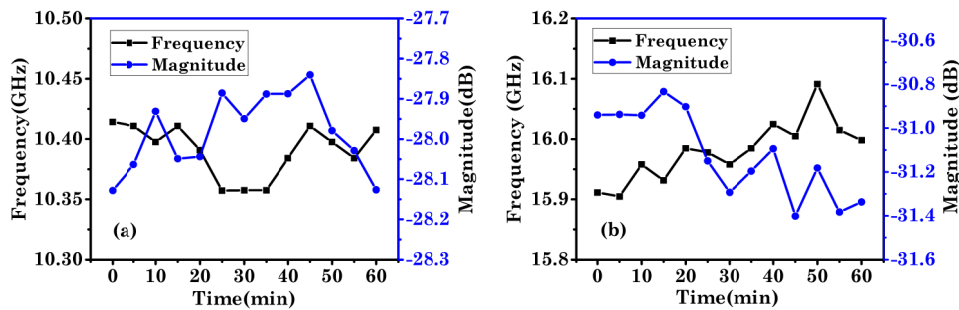


Fig. 8. The stability of the central frequency and magnitude of (a) the 1st passband and (b) the 2nd passband in 1 h with 5 min interval.

The stability of the proposed MPF is also studied. The central frequency and magnitude of the two passbands are measured every 5 minutes for 1 hour. In Fig. 8(a), the frequency and magnitude variations of the 1st passband centered around 10.4 GHz are less than  $\pm 29$  MHz

and  $\pm 0.14$  dB, respectively. The frequency and magnitude variations of the 2nd passband centered around 16.0 GHz are less than  $\pm 43$  MHz and  $\pm 0.27$  dB, respectively. The magnitude variations decrease significantly than [14] reported  $\pm 0.5$  dB. The stability of the 1st passband is better than the 2nd in two aspects because of the better wavelength stability of TL1, so we believe that the stability of the MPF can be further improved by using laser sources with dramatic performance [14].

#### 4.2 Single-passband

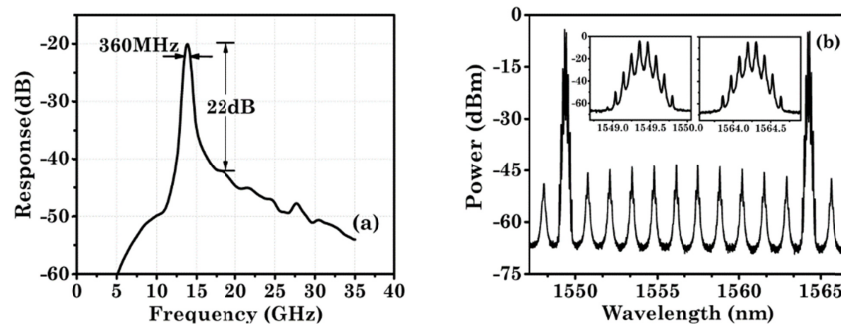


Fig. 9. The proposed single-passband MPF. (a) Measured amplitude response with the out-of-band suppression ratio of 22 dB and the 3-dB bandwidth of 360 MHz and (b) the corresponding optical spectra and enlarged view of insets.

In the experiment based on Fig. 2, a dual-passband MPF is implemented as the two wavelengths of two lights emitting from TL1 and TL2. Except for the multiple-passband MPF with two passbands, a single-passband MPF can also be obtained by fine-tuning the injection parameters [19]. In comparison with the single-passband MPF realized by one tunable laser source, the proposed method achieves high rejection ratio due to the overlapping between the two independent tunable passbands. Figure 9(a) shows the proposed single-passband MPF by two passbands overlapping with each other when  $I_b = 25.68$  mA,  $R_1 = 14.35$  dB,  $R_2 = 15.79$  dB,  $\Delta f_1 = 1.50$  GHz, and  $\Delta f_2 = 1.96$  GHz. The single-passband MPF is centered at 13.8 GHz, the peak power is  $-20.7$  dB and the 3-dB bandwidth is 360 MHz which are better than other implementations [3,28]. By calculation, the shape factor of the filter is 3.7 as a figure-of-merit indicating a notable selectivity [14].

Moreover, Fig. 9(b) shows the corresponding spectrum observed from OSA. There are multiple longitudinal modes in an FP cavity and the mode of the largest amplitude in the middle wavelength. Because of our instruments limitation, the wavelength of injection lights are only around the range of 1470~1550 and 1555~1575 nm, so the central wavelengths of the master lasers are 1549.360 and 1564.196 nm. As can be seen from Fig. 9(b), while external optical injection-locking, the FP laser is simulated amplification in the two modes (locked modes) and other longitudinal modes are suppressed by more than 40 dB. The insets are the zoom-in view of injection-locked mode which obtains great gain, and the spectrums of two passbands are almost the same. Moreover, the power of cavity mode is almost equal to that of carrier light, which represents the  $-1$ st order sideband obtains high conversion efficiency.

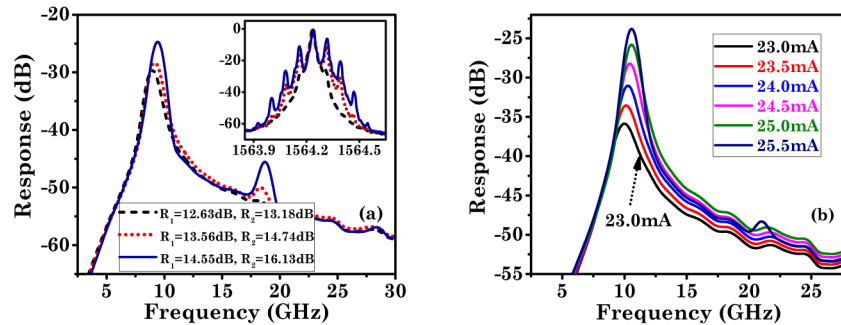


Fig. 10. (a) Measured amplitude responses of the single-passband MPFs realized with the different  $R_1$  and  $R_2$ . The inset is the corresponding spectrum. (b) Measured amplitude responses of the single-passband MPFs realized with the different  $I_b$ .

By adjusting the parameters of Eq. (4) and (5), the single-passband MPF also has the tunability. In Fig. 10(a), The bias current ( $I_b = 25.56$  mA) and detuning frequency ( $\Delta f_1 = 3.57$  GHz,  $\Delta f_2 = 3.70$  GHz) are unchangeable, while the larger injection ratio, the higher peak power, and the lower 3-dB bandwidth are changeable. It has been shown the regularity again that the central frequency and the magnitude of the passband are increased with the injection ratio, in accordance with Eq. (5) and similarly to the dual-passband. It is worth noting that there are two peaks in the response curves of red and blue lines, and the second peak stands for the amplification of + 1st order sideband [29]. According to the experimental results, the range edges are  $R_1 > 13$  dB and  $R_2 > 14$  dB. The generated response is tunable by controlling the bias current from 23.0 to 25.5 mA with a step of 0.5 mA as shown in Fig. 10(b). In contrast to the variation of magnitude, the resonance frequency increases with the increment of  $I_b$  like Fig. 7(a). Because the bandwidth of MPF is determined by the bandwidth of the gain at one longitudinal mode of the FP laser, the 3-dB bandwidth can be reduced as increasing the bias current [20]. However, when the + 1st order sideband nears to the slave laser mode, the interaction between the two modes leads to the second peak and the central frequency decrease.

## 5. Conclusions

We have demonstrated a novel multiple-passband microwave photonic filter with wide tunable frequency based on an injection-locked Fabry-Perot laser. In our proposed MPF, due to the frequency-selection effects caused by the structure of laser under multiple optical sources, the multiple passbands can be easily generated. The experiment incorporating two TLs has demonstrated the MPF function including both dual-passband and single-passband. We discuss the variation regularity between the frequency response and the injection parameters. By adjusting these parameters, the dual-passband MPF achieves the central frequency tuning range of 17 GHz and the out-of-band suppression of 24.1 dB. The single-passband MPF achieves the 3-dB bandwidth of 360 MHz, the shape factor of 3.7 and the insertion loss of 22 dB. In the experiment, we investigate the stability as well as the dynamic range of the dual-passband MPF, and its central and detuning frequency as a function of the injection ratio. The MPF based on injection locking has the potential for multiple microwave photonic applications such as high performance OEO, low and stable transmitters for WDM-PON and optical single-sideband modulation. We foresee continuous improvements in both bandwidth and resonance frequency when wide tunable sources are implemented, or by engineering and optimizing the slave laser for superior injection-locking performance.

## Funding

Chinese National Key Basic Research Special Fund (2017YFA0206401); Jiangsu Provincial Key Research and Development Plan (BE2017003-1); Jiangsu Overseas Visiting Scholar

Program for University Prominent Young & Middle-aged Teachers and Presidents; Qing Lan Project of Jiangsu Province.

## References

1. J. Capmany and D. Novak, "Microwave photonics combines two worlds," *Nat. Photonics* **1**(6), 319–330 (2007).
2. J. Yao, "Microwave Photonics," *J. Lightwave Technol.* **27**(3), 314–335 (2009).
3. H. S. Wen, M. Li, W. Li, and N. H. Zhu, "Ultrahigh-Q and tunable single-passband microwave photonic filter based on stimulated Brillouin scattering and a fiber ring resonator," *Opt. Lett.* **43**(19), 4659–4662 (2018).
4. O. Xu, J. Zhang, H. Deng, and J. Yao, "Dual-frequency optoelectronic oscillator for thermal-insensitive interrogation of a FBG strain sensor," *IEEE Photonics Technol. Lett.* **29**(4), 357–360 (2017).
5. R. Liao, M. Tang, S. Fu, and D. Liu, "Distributed measurement of polarization mode coupling in polarization maintaining fibers using microwave photonic filter technique," *J. Lightwave Technol.* **36**(19), 4543–4548 (2018).
6. L. Liu, F. Jiang, S. Yan, S. Min, M. He, D. Gao, and J. Dong, "Photonic measurement of microwave frequency using a silicon microdisk resonator," *Opt. Commun.* **335**, 266–270 (2015).
7. J. Xiong, R. Wang, T. Pu, T. Fang, J. Zheng, D. Chen, L. Huang, and X. Chen, "A novel approach to realizing a widely tunable single passband microwave photonic filter based on optical injection," *IEEE J. Sel. Top. Quantum Electron.* **21**(6), 171–176 (2015).
8. L. Huang, D. Chen, F. Zhang, P. Xiang, T. Zhang, P. Wang, L. Lu, T. Pu, and X. Chen, "Microwave photonic filter with multiple independently tunable passbands based on a broadband optical source," *Opt. Express* **23**(20), 25539–25552 (2015).
9. H. Chen, Z. Xu, H. Fu, S. Zhang, C. Wu, H. Wu, H. Xu, and Z. Cai, "Switchable and tunable microwave frequency multiplication based on a dual-passband microwave photonic filter," *Opt. Express* **23**(8), 9835–9843 (2015).
10. L. Gao, J. Zhang, X. Chen, and J. Yao, "Microwave photonic filter with two independently tunable passbands using a phase modulator and an equivalent phase-shifted Fiber Bragg Grating," *IEEE Trans. Microw. Theory Tech.* **62**(2), 380–387 (2014).
11. Y. Jiang, P. Shum, P. Zu, J. Zhou, G. Bai, J. Xu, Z. Zhou, H. Li, and S. Wang, "A selectable multiband bandpass microwave photonic filter," *IEEE Photonics J.* **5**(3), 5500509 (2013).
12. X. Han, E. Xu, W. Liu, and J. Yao, "Tunable dual-passband microwave photonic filter using orthogonal polarization modulation," *IEEE Photonics Technol. Lett.* **27**(20), 2209–2212 (2015).
13. K. P. Jackson, S. A. Newton, B. Moslehi, M. Tur, C. C. Cutler, J. W. Goodman, and H. J. Shaw, "Optical fiber delay-line signal processing," *IEEE Trans. Microw. Theory Tech.* **33**(3), 193–210 (1985).
14. J. Mora, B. Ortega, A. Diez, J. L. Cruz, M. V. Andrés, J. Capmany, and D. Pastor, "Photonic microwave tunable single-bandpass filter based on a Mach-Zehnder interferometer," *J. Lightwave Technol.* **24**(7), 2500–2509 (2006).
15. H. Wang, J. Y. Zheng, W. Li, L. X. Wang, M. Li, L. Xie, and N. H. Zhu, "Widely tunable single-bandpass microwave photonic filter based on polarization processing of a nonsliced broadband optical source," *Opt. Lett.* **38**(22), 4857–4860 (2013).
16. E. Xu, S. Pan, Z. Zhang, and P. Li, "Performance-improved microwave photonic single-passband filter using birefringence of phase-shifted fiber Bragg grating," *Opt. Commun.* **428**(1), 41–46 (2018).
17. N. Shi, T. Hao, W. Li, N. Zhu, and M. Li, "A reconfigurable microwave photonic filter with flexible tunability using a multi-wavelength laser and a multi-channel phase-shifted fiber Bragg grating," *Opt. Commun.* **407**(15), 27–32 (2018).
18. S. Pan and J. Yao, "Wideband and frequency-tunable microwave generation using an optoelectronic oscillator incorporating a Fabry-Perot laser diode with external optical injection," *Opt. Lett.* **35**(11), 1911–1913 (2010).
19. Y. Yu, J. Dong, E. Xu, X. Li, L. Zhou, F. Wang, and X. Zhang, "Single passband microwave photonic filter with continuous wideband tunability based on electro-optic phase modulator and Fabry-Pérot semiconductor optical amplifier," *J. Lightwave Technol.* **29**(23), 3542–3550 (2011).
20. F. Jiang, Y. Yu, H. Tang, L. Xu, and X. Zhang, "Tunable bandpass microwave photonic filter with ultrahigh stopband attenuation and skirt selectivity," *Opt. Express* **24**(16), 18655–18663 (2016).
21. Y. Cao, D. Xu, L. Chen, Z. Tong, and J. Yang, "Widely tunable microwave photonic filter based on four-wave mixing," *Opt. Eng.* **56**(2), 026110 (2017).
22. H. Sung, E. K. Lau, and M. C. Wu, "Optical single sideband modulation using strong optical injection-locked semiconductor lasers," *IEEE Photonics Technol. Lett.* **19**(13), 1005–1007 (2007).
23. A. Murakami, K. Kawashima, and K. Atsuki, "Cavity resonance shift and bandwidth enhancement in semiconductor lasers with strong light injection," *IEEE J. Quantum Electron.* **39**(10), 1196–1204 (2003).
24. R. Lang, "Injection locking properties of a semiconductor laser," *IEEE J. Quantum Electron.* **18**(6), 976–983 (1982).
25. F. Mogensen, H. Olesen, and G. Jacobsen, "Locking conditions and stability properties for a semiconductor laser with external light injection," *IEEE J. Quantum Electron.* **21**(7), 784–793 (1985).
26. W. E. Lamb, "Theory of an optical maser," *Phys. Rev.* **134**(6A), A1429–A1450 (1964).
27. R. Goto, T. Goto, N. Nishizawa, H. Kasuya, M. Mori, and K. Yamane, "Sideband injection locking using cavity-enhanced highly non-degenerate four-wave mixing in DFB-LDs," *Electron. Lett.* **34**(23), 2249–2250 (1998).

28. H. Zhu, R. Wang, P. Xiang, T. Pu, J. Zheng, Y. Li, T. Fang, L. Huang, Y. Han, and X. Chen, "Microwave photonic bandpass filter based on carrier-suppressed single sideband injected distributed feedback laser," *IEEE Photonics J.* **9**(3), 1–12 (2017).
29. J. Xiong, R. Wang, T. Pu, L. Lu, T. Fang, Z. Wei, G. Sun, J. Zheng, and P. Xiang, "A novel approach to realizing SSB modulation with optimum optical carrier to sideband ratio," *IEEE Photonics Technol. Lett.* **25**(12), 1114–1117 (2013).